Journal of Power Sources 328 (2016) 271–279

Contents lists available at ScienceDirect

Journal of Power Sources

journal homepage: www.elsevier.com/locate/jpowsour

Easy synthesis approach of Pt-nanoparticles on polyaniline surface: an efficient electro-catalyst for methanol oxidation reaction

Sanjoy Mondal, Sudip Malik*

Polymer Science Unit, Indian Association for the Cultivation of Science, 2A & 2B Raja S.C. Mullick Road, Jadavpur, Kolkata 700032, India

HIGHLIGHTS

- Decoration of Pt-nanoparticles on the polyaniline nanotubes (BDP@Pt).
- Synthesized BDP@Pt act as an efficient electro-catalyst for MOR in acidic medium.
- Efficiency and CO-tolerance ability depends with Pt-NPs density on PANI surface.

GRAPHICAL ABSTRACT

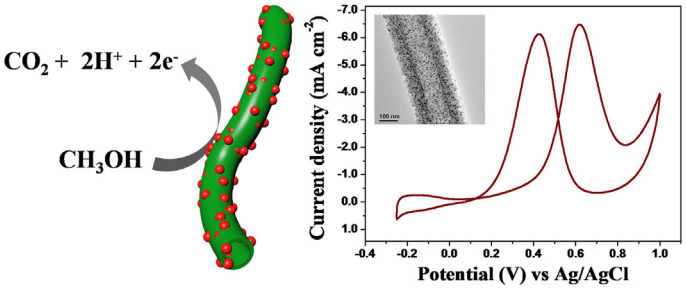

ARTICLE INFO

Article history:
Received 12 April 2016
Received in revised form
3 August 2016
Accepted 4 August 2016
Available online 12 August 2016

Keywords:
Polyaniline
Pt-nanoparicles
Easy synthesis
Methanol electro-oxidation
CO-tolerance

ABSTRACT

A facile room temperature and surfactant free synthesis of platinum nanoparticles (Pt-NPs) on benzene tetra-carboxylic acid doped polyaniline (BDP) tube has been successfully demonstrated by solution dipping method. Preparation of Pt-NPs has been done through a red-ox reaction between BDP tubes and Pt-salt, as BDP itself acts as nontoxic reducing agent as well as template cum stabilizer for Pt-NPs. In BDP@Pt composites, ~2.5 ± 0.5 nm spherical shaped Pt-NPs as observed from TEM studies are nicely decorated on the surface of BDP. The population or the loading density of Pt-NPs on BDP tube is greatly controlled by changing the w/w ratio of BDP to H_2PtCl_6. Synthesized BDP@Pt composites are subsequently employed as an efficient electro-catalyst for methanol oxidation reaction (MOR) in acidic medium. Furthermore, the observed catalytic activity is consequently ~12 times higher than that of commercially available Pt/C catalyst. Depending on the loading density of Pt-NPs on BDP tubes, the efficiency and carbon monoxide (CO) tolerance ability of composites have been explored.

1. Introduction

Direct methanol fuel cells (DMFCs) have received significant attention as a new portable clean power sources ranging from mobile phone to vehicles [1–5]. This considerable interest towards methanol is due to its high theoretical energy conversion efficiency, low pollutant emission, low materials cost, easy handle, simple storage, low temperature operation and many others [3,6,7]. However, some difficulties or drawbacks are still present for the commercialization of DMFCs including insufficient activity and high cost of anode modified materials. Pt-nanoparticles (Pt-NPs) are still regarded as most effective catalyst in the methanol oxidation reaction (MOR) than other metal nanomaterials (like Au, Ag, Pd, Ru *etc.*). However, the limited abundance and the high cost of Pt based materials make immense challenge for the scientists or researchers to produce easy, novel and smart method of

* Corresponding author.
E-mail address: psusm2@iacs.res.in (S. Malik).

http://dx.doi.org/10.1016/j.jpowsour.2016.08.026
0378-7753/

preparation [8–10]. Secondly, difficulty lies in the catalyst poisoning originated from the strong interaction of intermediate carbon monoxide (CO) species with catalyst active sites [11–14]. Thirdly, methanol crossover in electrolyte is sluggish the kinetics of methanol oxidation [15,16]. Therefore, the development of high CO-tolerance with excellent catalytic activity and good durability of electrochemical anodic material is the key issue nowadays. To address these concerns, tremendous efforts have been devoted by researchers to develop of Pt-NPs combine composites materials in which the size and shape of nanoparticles play an important role towards the methanol oxidation [17,18]. Ultrafine size Noble metal nanoparticles are more essential because of high surface areas, more edges and corners that cumulatively enhance the efficiency of the catalyst [19,20].

In general, Pt-NPs is most familiar efficient electro-catalytic material for methanol oxidation reaction. Many processes have been already well developed to making Pt-NPs with the help of several stabilizing and reducing agents. General approach is the chemically synthesized Pt-NPs that are subsequently stabilized by surfactants or any organic binders. These stabilizers fully or partially hinder the active site of catalyst, it results the lowering of catalytic efficiency and it is not suitable to use repeated times for catalytic cycles. Different carbon based materials like graphene [21–24], carbon nanotubes [25,26], carbon nanofibers [27,28], carbon black [29,30], mesoporous carbon [31] are utilized as supports for Pt-NPs in fuel cells. A number of bimetallic nanoparticles have been also developed for active anode materials in methanol fuel cell [5,32,33]. Majority of Pt-NPs based composite materials have prepared through different reaction condition, like high reaction temperature, hazardous reagent used, multistep reaction procedure, lack of purification *etc*. and it is less demanding from the view point of applications. Therefore, making of single step, eco-friendly, easy, high performance, cost effective Pt-based electro-catalyst with high durability and CO tolerance ability is still missing in the literature.

Currently, polymer-Pt nanocomposites have received a great deal of attention owing to their excellent chemical and physical properties in the fields of catalysis, electronic devices, solar cell, sensor *etc*. In the conducting polymer family, polyaniline (PANI) is the most popular polymer and significant for the formation of metal-incorporated nanostructure, because (i) the presence of amine (–NH–) moiety in the main polymer chain that helps chemically synthesized Pt-NPs attached on PANI surface by electrostatic interaction [34–37]. (ii) The crucial advantage of PANI for its reduction potential (0.70–0.75 V) [38], which is relatively higher than that of the common noble metal, (Au, Ag, Pd, Pt) and it results the facile formation of metal nanoparticles at room temperature [39,40]. (iii) Reducing nature of PANI chain to form metal nanoparticles unlike other conductive polymers. (iv) A good solid support cum template material for metal NPs. (v) PANI itself interacts with water molecule and it may facilitate the oxidation of CO to CO_2 during methanol oxidation reaction at room temperature [41–43]. (vi) Apart from these, easy synthesis procedure, low materials production cost, good thermal as well as environmental stability, high electrical conductivity, doping/dedoping behaviour of PANI makes signification advantages in research field [44,45].

In this article, we have reported an easy and room temperature procedure for synthesis of Pt-NPs, embellished on high aspect ratio benzene tetra-carboxylic acid doped polyaniline (BDP) nanotube, that behaves as a reducing template cum solid supporting agent for Pt-NPs. Synthesized BDP@Pt composites have been characterized by TEM, XPS, XRD, ICP-AES studies. The population density of Pt-NPs on PANI surface has been checked with changing BDP to Pt w/w ratio although shape and size of Pt-NPs remains almost same. Prepared surfactant free Pt-NPs on BDP tubes have been utilized as efficient electro-catalysts for methanol oxidation reaction. The ratio of BDP to Pt (w/w) has been optimized as an efficient and CO-tolerance composite for methanol oxidation reaction at room temperature. CO-tolerance activity has been also compared with the commercially available Pt/C catalyst.

2. Experimental section

2.1. Materials

Aniline and methanol were supplied by Merck Chemicals. Aniline was distilled under reduced pressure and stored at 5 °C in a dark place and methanol (CH_3OH) was distilled under normal pressure in N_2 atmosphere. Chloroplatinic acid hexahydrate (H_2PtCl_6, $6H_2O$, ≥37.50% Pt basis), Pt/C (10% wt. loading), 1,2,4,5-benzene tetra-carboxylic acid (BTCA), and ammonium persulfate-persulfate [$(NH_4)_2S_2O_8$] (APS) were purchased from Sigma-Aldrich and were used without further purification. All solutions were prepared in deionised water (18 MΩ cm, Millipore Milli Q water).

2.2. Preparation of 1,2,4,5-benzene tetra-carboxylic acid doped polyaniline (BDP)

1,2,4,5-benzene tetra-carboxylic acid doped polyaniline (BDP) was synthesized according to our early report [37]. In the typical experiment, BTCA (0.07 g, 0.27 mmol) was dissolved in 15 mL of water with continuous stirring. Aniline (100 μL, 1.02 gcm^{-3}, 1.1 mmol) was added to 15 mL BTCA soluble water solution and stirred for another 1 h at 25 °C. A fresh aqueous solution of APS was added drop by drop to the reaction mixture at 10 °C and reaction mixture was allowed to stand at 5 °C temperature for 18 h without stirring. The deep green color precipitate was washed several times with water followed by methanol to remove the oligomers and excess APS. Finally, the solid product was dried at 80 °C under vacuum to get high-aspect-ratio BTCA-doped PANI (BDP) tubes as powdered form.

2.3. Preparation of the BDP@Pt catalyst

The Scheme 1 illustrated the fabrication of Pt-NPs on BDP fiber. In the typical experiment 1.0 mg of BDP fiber was dispersed in 500 μL of water in a glass bottle equipped with magnetic stirrer. In different sets of batch reaction (Table 1) 3.5 mL of H_2PtCl_6 solution with four different concentration (0.25, 0.5, 0.75 and 1.0 mg mL^{-1}) were added drop wise with continuous stirring for 24 h at room temperature (25 °C) until to complete reduction. Synthesized BDP@Pt composite was collected by centrifugation at 5000 rpm and thoroughly washes with pure water several times. Finally, prepared composites were purified through dialysis processes (2000 MW cut off) to remove untreated H_2PtCl_6 from the surface. Resulting composites were used as stock materials for further experiments.

2.4. Characterization

Material characterizations were performed with the help of following technique and instruments. Bright-field, high-angle annular dark-field (HAADF) imaging and mapping of BDP@Pt composites were carried out on a UHR-FEG-TEM (JEOL, JEM 2100 F) instrument at an accelerating voltage of 200 kV. Prior to TEM observation, samples were dispersed in water and soaked with a 200 mesh carbon film coated Cu-grid. FESEM study was done by JEOL, JSM 6700 F instrument operating at 5 kV, a small amount of water dispersed sample was drop casted on a glass cover slip and dried at room temperature. XRD analysis were performed through Bruker AXS diffractometer (D8 advance) using Cu Kα radiation

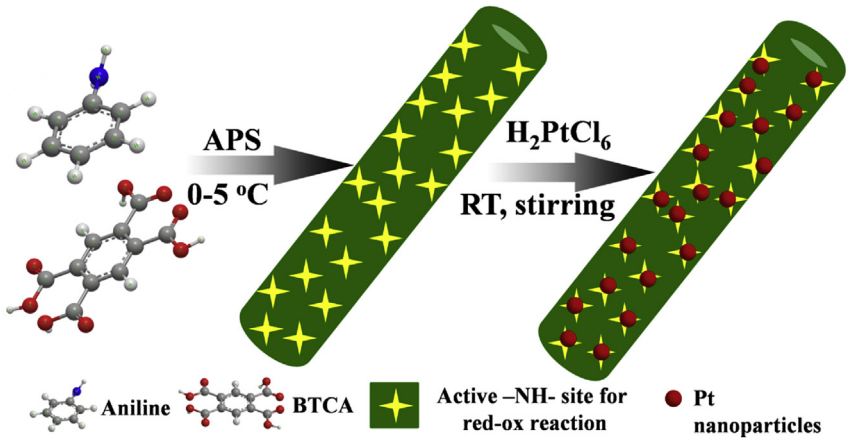

Scheme 1. Schematic presentation for the preparation of BDP@Pt composites.

Table 1
Preparation of different Pt-NPs loading % BDP@Pt composite and their electro-catalytic activity.

Composite	BDP (mg)	H_2PtCl_6 (mg)	BDP:Pt (w/w)	Pt loading %	Pt NPs		ECSA (m^2g^{-1})	*If/Ib*[b]	
					Shape	*Size (nm)*		*(Initial cycle)*	*100thcycle*
Pt/C[a]	-	-	–	10.0	Spherical	2.3 to 3.0	14.62	–	–
BDP@Pt1	10.00	8.75	1:0.8	12.5	Spherical	2.5 ± 0.5	20.47	1.81	1.54
BDP@Pt2	10.00	17.5	1:1.7	29.1	Spherical	2.5 ± 0.5	38.63	1.14	1.01
BDP@Pt3	10.00	26.2	1:2.6	42.2	Spherical	2.5 ± 0.5	62.60	1.05	0.99
BDP@Pt4	10.00	35.0	1:3.5	61.5	Spherical	2.5 ± 0.5	69.54	1.09	0.86

[a] Data were taken from the catalogue of commercial supplier.
[b] The ratio of forward and backward peak intensity of methanol oxidation reaction.

($\lambda = 1.542$ Å), a generator voltage of 40 kV, and a current of 40 mA. Powder samples were scanned from $2\theta = 10–85^\circ$ at the rate of 0.5 s per step with a step width of 0.02. XPS study was completed by using a focused monochromatized Al Kα X-ray source (1486.8 eV) in an Omicron Nano Technology 0571 XPS instrument. The amount of Pt present in the BDP@Pt composites were measured by an Optima 2100 DV (PerkinElmer) inductively coupled plasma atomic-emission spectroscopy (ICP-AES) instrument. UV–vis spectra of BDP fiber were recorded from Agilent (model 8453) a UV–vis spectrophotometer by using a quartz cell with path length of 1.0 cm. FTIR studies were carried out in Shimadzu instrument (FTIR-8400 S) using KBr pellets.

2.5. Electrochemical measurements

All electrochemical experiments like cyclic voltammetry (CV), electrochemical impedance spectroscopy (EIS) and chrono-noamperometry (CA) were performed by a CHI6087E electrochemical workstation (CHI, USA). A conventional three-electrode cell setup was used for these experiments, which consisted of a BDP@Pt composites modified glassy carbon electrode (GCE) as a working electrode, a Pt-wire as an auxiliary electrode, a saturated Ag/AgCl as a reference electrode. GCE of 3 mm in diameter (0.07 cm^2 surface area) was polished very carefully with 1, 0.3, and 0.05 μm alumina powder step by step, until a mirror finish was obtained. GCE was washed with water and ethanol mixture several times and dried in air at room temperature. The water dispersed synthesized BDP@Pt composite was dropped over on active surface of GCE and dried under N_2 atmosphere at room temperature for further electrochemical measurement. The electro-oxidation of methanol was recorded by cyclic voltammetry technique at scan rate 50 mV^{-1} in a mixture of 0.5 M H_2SO_4 and 0.5 M methanol. Current per geometrical surface area (current density) was used for all calculation except the catalytic activity towards MOR, current per ECSA was considered.

CO-stripping voltammetry experiment was performed by same electrochemical experimental setup. BDP@Pt composite modified working electrode was feeding with CO gas externally for 10 min bubbling. After the adsorption on Pt-NPs surface, CO was eliminated from electrode surface through dry N_2 bubbling for 30 min. The CO stripping voltammogram was recorded at room temperature with 50 mV^{-1} scan speed.

3. Result and discussion

3.1. Morphological study

Chemical synthesis of BDP are schematically shown in Fig. 1a and prepared BDP are hollow tube having diameter ~200 nm as observed in FESEM investigations (Fig. 1b). The careful observation of TEM image proves tube like morphology judged from contrast different between edge and core of fiber (Fig. 1c). After treatment of BDP tubes with H_2PtCl_6, Pt-NPs are formed in/on BDP surface. Four different BDP@Pt composites have been synthesized with different w/w ratio of BDP to H_2PtCl_6 salt.

TEM images of BDP@Pt composites (Fig. 2) reveal the tubular structures of PANI and interaction of BDP tubes with the tiny Pt-NPs. It is also seen that Pt-NPs are embedded on the surface of BDP tube without affecting the BDP morphology. The very close look of TEM image shows, Pt-NPs are tightly adhered to the BDP surface without large aggregates, indicating the strong interaction between the Pt-NPs and the BDP solid support and the reduction of Pt ions by PANI chains. The loading density of Pt-NPs on BDP surface is controlling by changing the w/w ratio of BDP to H_2PtCl_6 (Table 1). The loading density estimated by ICP-AES measurement is 61.5, 42.2, 29.1, and 12.5 wt % for BDP@Pt4, BDP@Pt3, BDP@Pt2 and

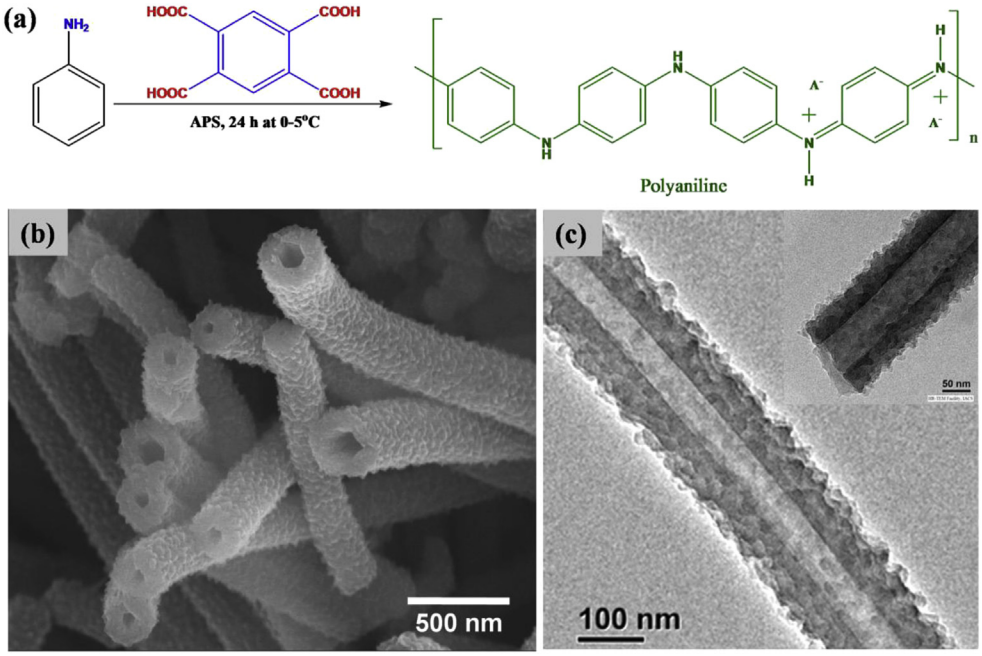

Fig. 1. (a) Preparation of BDP, (b) FESEM image and (c) TEM image of synthesized BDP fiber showing tube like nature.

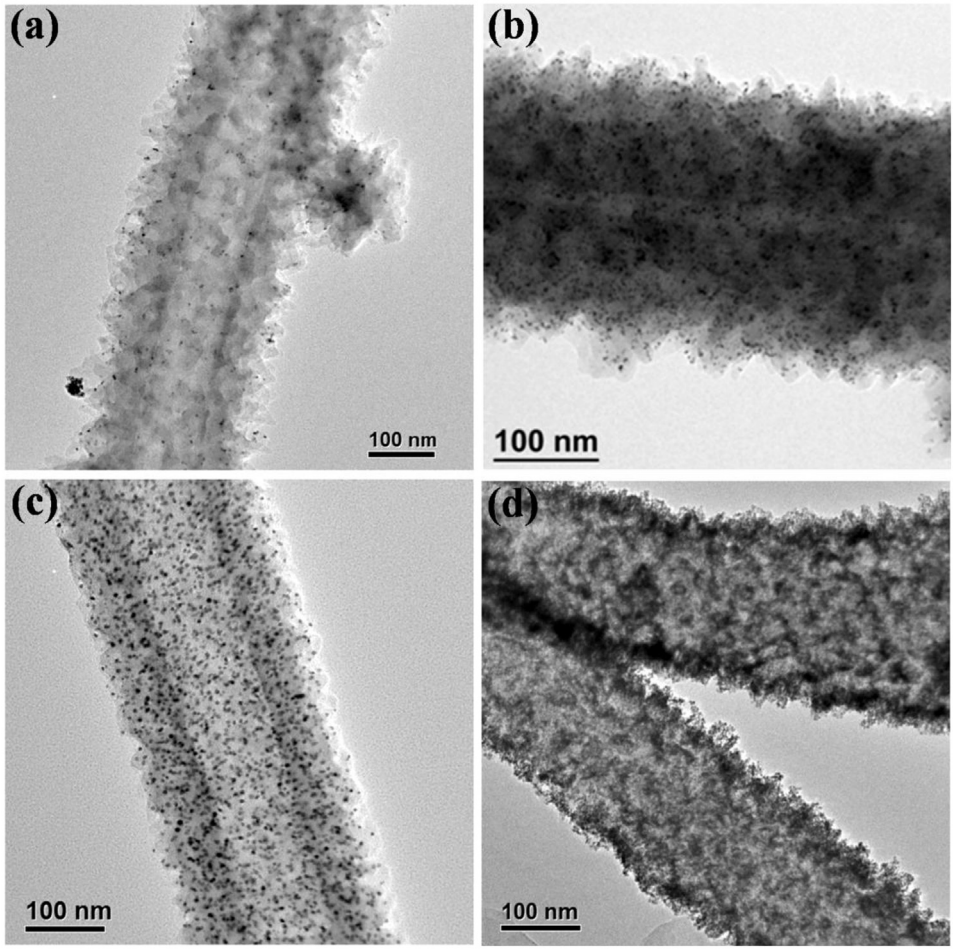

Fig. 2. TEM images of room temperature synthesized Pt-NPs decorated BDP nanotube with different BDP to H_2PtCl_6 w/w ratio (a) BDP@Pt1; (b) BDP@Pt2; (c) BDP@Pt3; (d) BDP@Pt4

BDP@Pt1, respectively. The maximum Pt-NPs loading density is achieved in BDP@Pt4 composite, where BDP to H_2PtCl_6 w/w ratio is 1:3.5. However the particles size remains almost same ~2.5 ± 0.5 nm in all composites (Fig. S3).

Careful observation of high magnification TEM image of BDP@Pt3 composite clearly shows that dark black spots are Pt-NPs, that are uniformly distributed over on BDP tubes (Fig. 3a). The close look of TEM image (Fig. 3b) of BDP@Pt3 composite indicates that BDP tubes are coated by tiny Pt-NPs that is also confirmed from dark field image (Fig. 3c). A selected region of TEM image is used to determine particle size distribution and histogram of Pt-NPs. The size of Pt-NPs is quite uniform (~2.5 ± 0.5 nm), although shapes of the particles are not exactly spherical in nature (Fig. S2). The layer to layer distance of single Pt-NPs is calculated ~0.225 nm, from high resolution fringe lattice image (inset image of Fig. 3b). SAED pattern (inset image of Fig. S2b) exactly matches with (111) plane of Pt-NPs in XRD study [9,24,46]. The presence of Pt-NPs on BDP fiber confirms from the mapping image by yellow coloring (Fig. 3e) of the selected area of Fig. 3d. The EDX study of BDP@Pt composite reveals that it consists of Carbon, Nitrogen, Oxygen and Platinum (Fig. 3f) environment.

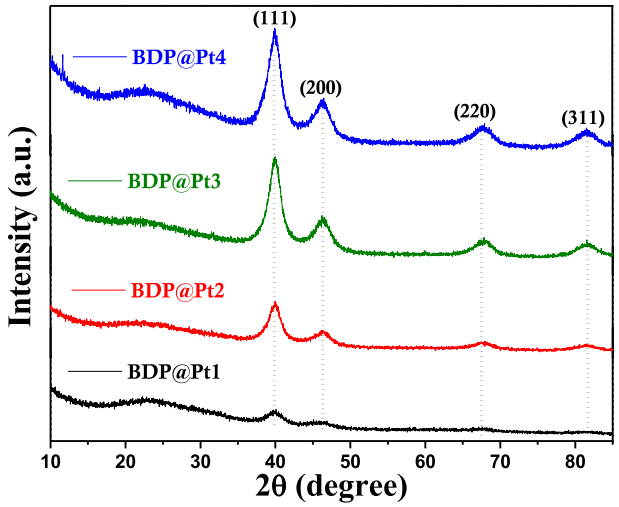

Fig. 4. Powdered XRD pattern of BDP@Pt1 composite (black), BDP@Pt2 composite (red) BDP@Pt3 composite (green), BDP@Pt4 composite (blue). (For interpretation of the references to colour in this figure legend, the reader is referred to the web version of this article.)

3.2. XRD study

X-ray diffraction (XRD) patterns of BDP@Pt composites in the range of 2θ = 10-85° show the presence of amorphous PANI and crystalline Pt-NPs (Fig. 4). A broad peak at ~15-30° indicates for the amorphous nature of PANI [37,45,47] and other four strong peaks for crystalline Pt-NPs. Strong crystalline peaks centered at 2θ = 40°, 46.3°, 67.8° and 81.5° correspond to (111), (200), (220) and (311) crystal planes of the fcc Pt-NPs [33,48,49]. XRD results suggest that Pt species are reduced to the metallic state of nanoparticles embedded in PANI supported matrix. The intensity of diffraction peak for Pt-NPs is increased from BDP@Pt1 to BDP@Pt4 composite with the increase of the loading density of Pt-NP over on PANI matrix. The fringe distance *i.e.*, layer to layer distance between two similar crystal plane of metal has been calculated from Bragg's equation: $n\lambda = 2dsin\theta$, where, "λ" indicates X-ray wavelength (Cu K_α = 0.154 nm), "d" is the layer to layer distance between two similar crystal plane, "θ" stands for Bragg angle (°). The calculated fringe distance from Bragg's equation for (111) crystal planes is ~0.225 nm which is matched with TEM result (inset image of Fig. 3b and Fig. S2b) [9,24,46].

3.3. XPS study

To analyze the chemical composition of BDP@Pt3 composite, X-ray photoelectron spectroscopy (XPS) study has been further

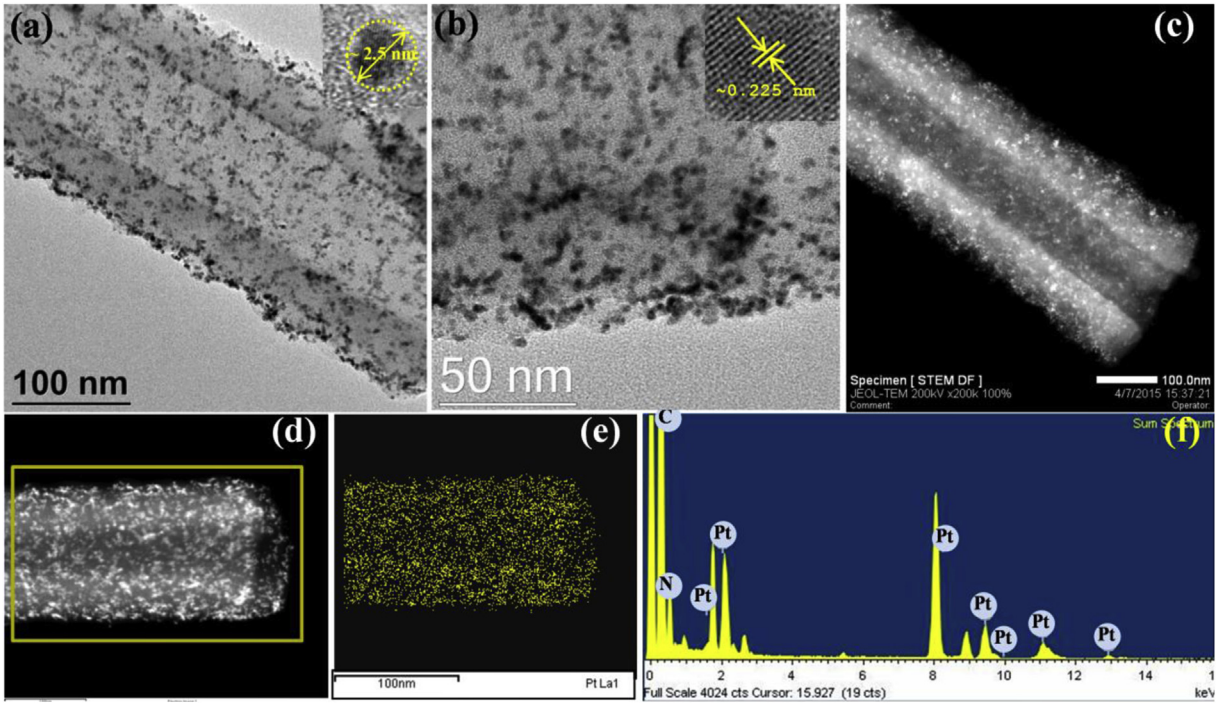

Fig. 3. (a) PANI nanofiber coated Pt-NPs; (b) HRTEM images with fringe pattern (inset image) of BDP@Pt3 composite; (c) Dark filed image; (d) dark field image with selected area for mapping; (e) corresponding mapping image; (f) EDX pattern of BDP@Pt3 composite.

employed in the region of binding energy (E_b) = 50–700 eV (Fig. 5). Full scanned XPS spectra reveal that composites consist of Carbon, Nitrogen, Oxygen and Platinum due to the presence of C1s, N1s, O1s and Pt4f signals at ~282, 397, 530 and 72 eV, respectively (Fig. 5a) [50,51]. In the region of E_b = 65–80 eV two strong signals at 69.7 and 72.6 eV correspond to $Pt4f_{7/2}$ and $Pt4f_{5/2}$ respectively (Fig. 5b).

The deconvoluted XPS spectra of Pt4f indicate the presence of three different oxidation state of platinum in the composite. Peaks at 69.5 and 72.6 eV are corresponding Pt are in metallic state *i.e.* Pt (0). Another two peaks at 70.2 and 73.4 eV are attributed to oxide Pt (II); again peaks at 72 and 74.2 eV are for oxide Pt (IV) [22]. Similarly, deconvoluted XPS spectra of N1s (Fig. 5c) reveal the information of three sub-peak at 396.5 (-N=), 397.6 (–NH–) and 398.3 eV for ($-N^+-$) [36,44,52]. The deconvoluted C1s spectrum shows three sub-peak at 281.3, 283.2 and 283.8 eV for C=C/C–C, C–N/C–O and C=O, respectively (Fig. 5d). Therefore, XPS studies suggest the presence of metal and metal oxide as a mixture along with C1s, N1s and O1s signal from PANI support.

3.4. Electro-catalytic oxidation of methanol

The electrochemical performances of prepared BDP@Pt composites (with different Pt-NPs loading density on BDP fiber) have been evaluated towards methanol oxidation reaction (MOR). Commercial available Pt/C (10% Pt loading) has been taken for comparison of MOR study. The cyclic voltammetry (CV) curve of prepared four BDP@Pt composites and commercial Pt/C recorded in 0.5 M H_2SO_4 solution at scan speed of 50 mV^{-1} are shown in Fig. 6.

The voltagram clearly provides the information about the hydrogen adsorption/desorption on the surface of BDP@Pt, oxide formation and oxide reduction on Pt-NPs surface of BDP@Pt composite. The higher potential peak at ~0.48 V is attributed to the reduction of Pt-oxide on BDP fiber surface during forward scan [22,53]. While characteristic peak at lower potential ~ –0.25 to 0.1 V region is attributed to monolayer hydrogen adsorption/desorption on Pt-NPs active surface [49,54,55]. The electrochemical surface area (ECSA) is an important parameter for electrochemical performance of an electro-catalyst. The ECSA of the BDP@Pt catalyst has been calculated from the coulombic charge of hydrogen

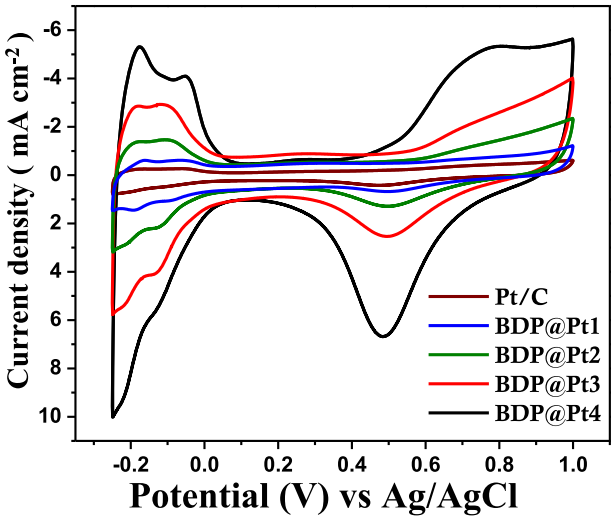

Fig. 6. Cyclic voltammograms of BDP@Pt composites in 0.5 M H_2SO_4 with scan speed 50 mV^{-1} at room temperature.

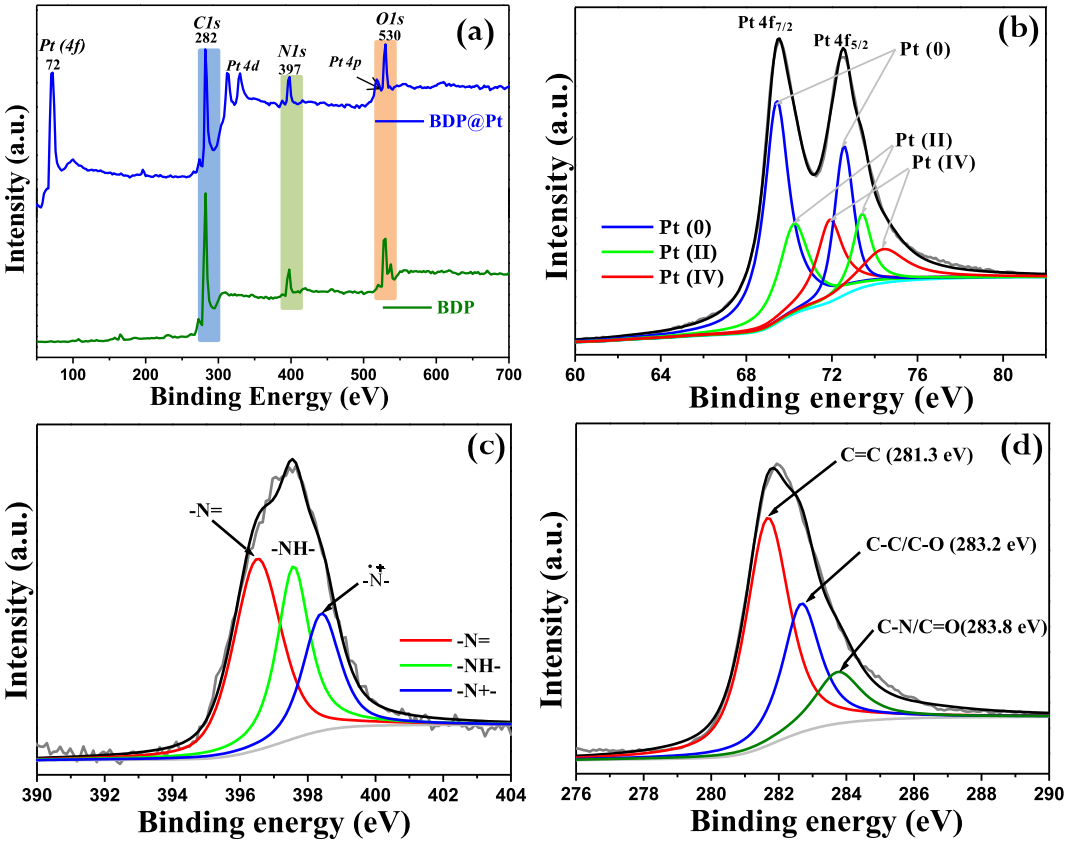

Fig. 5. (a) Full scan XPS study of BDP and BDP@Pt3 composite; (b) deconvoluted XPS spectra for Pt 4f; (c) deconvoluted XPS spectra of N1s; (d) deconvoluted XPS signature of C1s.

adsorption/desorption (Q_H) with respect to the value of 210 μCcm^{-2} for hydrogen monolayer formation on a smooth surface [56,57]. Integrated anodic and cathodic peak areas of hydrogen adsorption/desorption in the potential range −0.25 to 0.1 V (*vs* SCE) are directly associated to the Q_H. The ECSA of all BDP@Pt catalyst along with control has been calculated by following equation [21,22,49,58].

$$ECSA = \frac{Q_H}{m_{pt} \times 210 \times 10^{-6}}$$

where, 'Q_H' is the total charge relating to H^+ adsorption on integrated peak area of hydrogen adsorption/desorption; 'm_{Pt}' is the active mass of Pt catalyst (g m^{-2}) on the glassy carbon electrode and it is 0.807 g m^{-2} for BDP@Pt4, 0.485 g m^{-2} for BDP@Pt3, 0.686 g m^{-2} for BDP@Pt2, 1.143 g m^{-2} for BDP@pt1 and 1.56 g m^{-2} for Pt/C.

The calculated ECSA value for BDP@Pt composites (from BDP@Pt1 to BDP@Pt4, Table 1) are ~20.47 m^2 g^{-1}, 38.63 m^2 g^{-1}, 62.6 m^2 g^{-1}, and 69.54 m^2 g^{-1}, respectively. The ECSA value for BDP@Pt1 is 1.4 times, BDP@Pt2 is 2.7 times, BDP@Pt3 is 4.5 times and BDP@Pt4 is 5 times higher than that of commercial Pt/C catalyst. Calculated ECSA values imply the significant improvement of electrochemical activity on Pt-NPs site in the BDP@Pt composites.

CV curves for MOR by BDP@Pt composites (as an active electrocatalyst) are shown in Fig. 7. The oxidation reaction has been tested by BDP@Pt composites modified GCE in 0.5 M H_2SO_4 electrolyte solution containing 0.5 M methanol at 25 °C temperature with potential range −0.25–1.0 V (vs SCE). Voltamograms represent significantly different voltametric behaviours in terms of oxidation peak potential and specific activities. MOR consists of two well defined oxidation peaks at forward and reverse scan. The first one between 0.4 and 0.8 V in the forward scan and the second peak is between 0.1 and 0.6 V in the backward scan. The peak current density (current per ECSA) at the forward scan (I_f) corresponds to dehydrogenation of methanol oxidation and the oxidation of adsorbed species, producing Pt-adsorbed carboneous species such as CO. This Pt-adsorbed CO acts as catalyst poison. Methanol oxidation reactions on BDP@Pt surface are represented by the following reactions at forward peak:

$$BDP@Pt + CH_3OH \rightarrow BDP@Pt - (CH_3OH)_{ads}$$
$$BDP@Pt - (CH_3OH)_{ads} \rightarrow BDP@Pt - (CO)_{ads} + 4H^+ + 4e^-$$
$$BDP@Pt + H_2O \rightarrow BDP@Pt - (OH)_{ads} + H^+ + e^-$$

and at reverse peak:

$$BDP@Pt - (CO)_{ads} + BDP@pt - (OH)_{ads} \rightarrow BDP@Pt + CO_2 + H^+ + e^-$$

The peak current density at backward scan (I_b) is primarily associated with the oxidation of adsorbed carboneous species as an intermediate species that are not completely oxidised in the forward scan [4,58]. To distinguish the intrinsic activity of Pt active surface area from the activity caused by large Pt active surface area, we have compared the intensity of the peak current density of individual composite with commercial Pt/C. The intensity of peak current at forward scan (I_f) at 0.4–0.8 V of methanol oxidation for BDP@Pt4 composite is ~12 times, BDP@Pt3 is ~6 times, BDP@Pt2 is ~4 times and BDP@Pt1 composite ~2 times higher performance with respect to Pt/C catalyst by taking consideration of current per ECSA. Importantly, absolute value of I_f *or* I_b and the ratio of I_f/I_b are two crucial parameters which lead to the better understanding of catalytic efficiency as well as catalyst poisoning behaviour. Higher the value of peak current intensity will be the higher catalytic efficiency [30,59]. Values of I_f *or* I_b (initial cycle or 100th cycle) are gradually increased from BDP@Pt1 to BDP@Pt4. As higher value of I_f

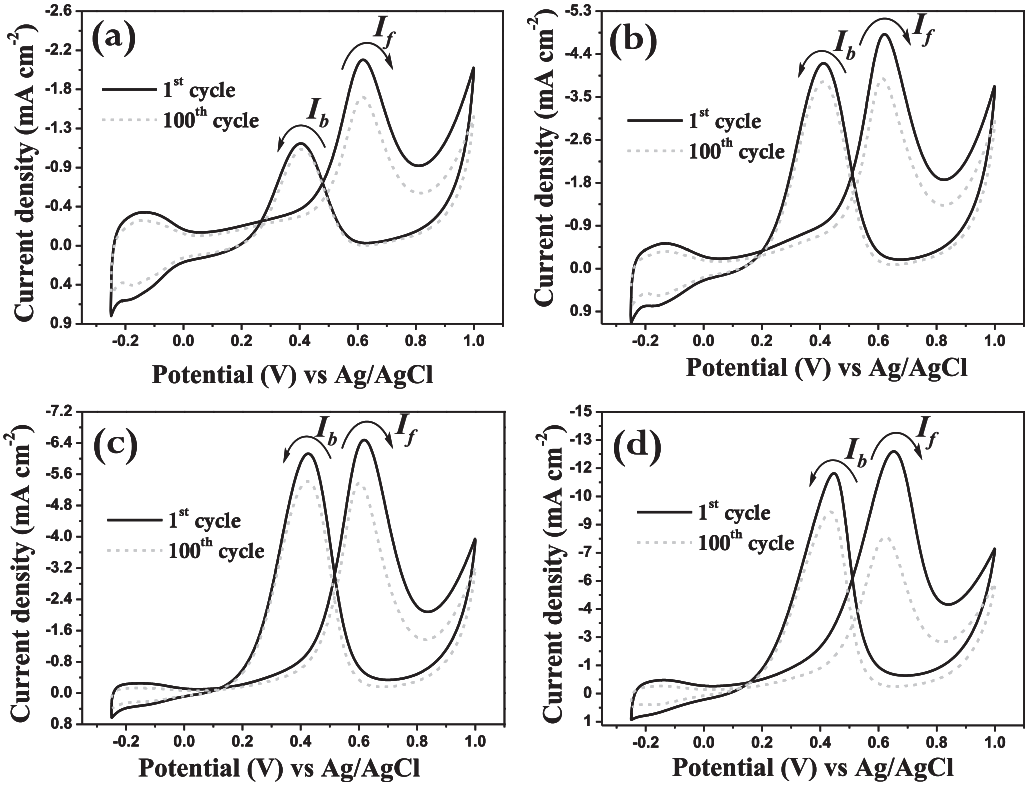

Fig. 7. Cyclic voltammetry curve MOR 1st cycle (black line) and 100th cycle (grey dot line) on BDP@Pt catalyst surface from mixture of 0.5 M methanol + 0.5 M H_2SO_4 in the potential range −0.25–1.0 V (vs SCE) with scan rate 50 mV^{-1} at 25 °C temperature (a) BDP@Pt1, (b) BDP@Pt2, (c) BDP@Pt3 and (d) BDP@Pt4. Arrows indicate the direction of scan.

or I_b is observed for BDP@Pt4, it is the efficient catalyst among four composites. In our MOR study, I_f/I_b (1st cycle or 100th cycle) ratio decreases with increasing ECSA from BDP@Pt1 to BDP@Pt4. The ratio of I_f/I_b decreases from 1st cycle to 100th cycle for a single composite. It means that after 100th cycle catalytic efficiency decreases. Interestingly, I_f/I_b ratio after 100th cycle is going down to 0.86 for BDP@Pt4 composite (Table 1), indicating higher catalyst poisoning for BDP@Pt4 than that of others three BDP@Pt composites. This type of catalyst poisoning may be explained from the morphology pattern of BDP@Pt4 composite. In BDP@Pt4 composites, BDP tubes are fully covered with Pt-NPs (Fig. 2d) and it reduces the vacant space required for the CO liberation. So with increasing Pt-NPs loading density as catalytic efficiency/activity increases and catalytic poisonability also increases. From the consideration of ECSA and I_f/I_b together, BDP@Pt3 composite is the best among the four synthesized materials as an efficient catalyst with comparable good catalytic efficiency and relatively low poisoning ability.

The long-term performance of catalyst towards methanol oxidation has been checked by the continued CV cycles and chronoamperometric (CA) study. The CA study of synthesized BDP@Pt composites and commercial Pt/C are represented in Fig. 8b. CA studies were conducted in 0.5 M H_2SO_4 solution containing 0.5 M methanol at 0.61 V for a period of 1200 s. Initially, chronoamperometric curves decay owing to the formation intermediate species such as BDP@Pt-$(CH_3OH)_{ads}$, BDP@Pt-$(CO)_{ads}$, BDP@Pt-$(OH)_{ads}$ *etc*. that are deactivating the Pt-surface. After a certain times, the rate of current decay gradually slows and remains at pseudo-steady value because of adsorption/desorption equilibrium of intermediate species on the surface [4].

The CO-tolerance ability is also estimated from the ratio of I_f and I_b, higher I_f/I_b ratio implies the better CO-tolerance that is complete oxidation methanol to CO_2 [57,60]. Lower I_f/I_b ratio suggests low CO-tolerance. The I_f/I_b ratio decreases from BDP@Pt1 to BDP@Pt4 composite (Table 1) which signifies CO-tolerance ability is decreased from BDP@Pt1 to BDP@Pt4 composite. To confirm CO tolerance ability of synthesized BDP@Pt composites, CO-stripping has been measured (Fig. 8c). In CO_{ads}-stripping experiment, peak at ~0.5–0.7 V has been observed after feeding the composite modified working electrode with CO gas externally for 10 min bubbling and the same peak is disappeared upon treatment with dry N_2 gas for 30 min. The obtained peak intensity is much higher for BDP@Pt4 composite than other three BDP@Pt composites. It indicates that BDP@Pt4 composite is highly affected by CO as a reaction intermediate species in MOR though it shows relatively higher catalytic ECSA compared to BDP@Pt3. Benzene tetracarboxylic acid plays a very important role to achieve high aspect ratio polyaniline tubes [37]. Subsequently, Pt ions are reduced to Pt-NPs by polyaniline chains (without use of any external reducing agents). These tubes are: (a) generating more surface area on which Pt-NPs reside, (b) inhibiting the agglomeration of Pt-NPs, (c) maintaining nice distribution of Pt-NPs on/into PANI matrix of BDP fibers and (d) facilitating the diffusion of methanol to Pt-NPs for catalytic activity. Moreover, PANI tube also assists to CO-tolerance ability in MOR as amine groups of PANI chains and carboxylic functional group of benzene tetra-carboxylic acids help to adsorb water molecule to form BDP@Pt-$(OH)_{ads}$ that accelerates the

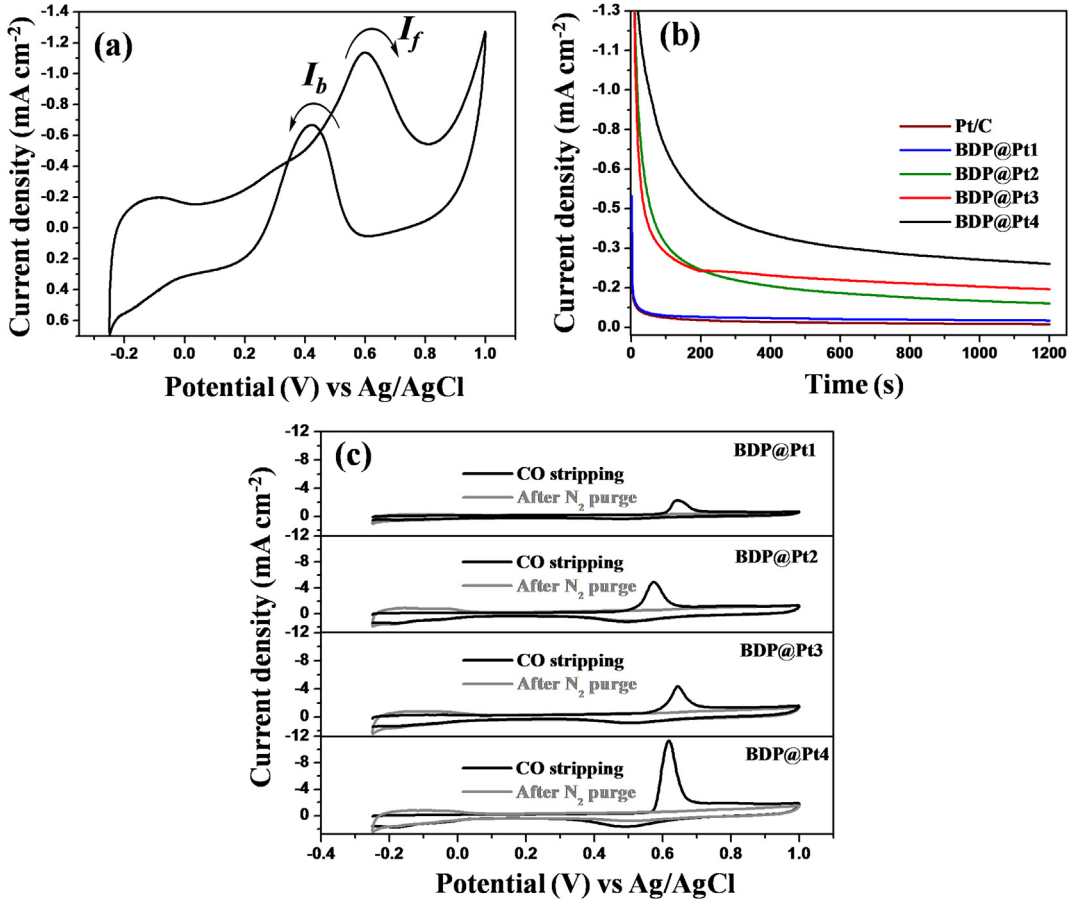

Fig. 8. (a) MOR study by commercial Pt/C catalyst with scan speed 50 mV^{-1}; Chrono-amperometric study of synthesized BDP@Pt composite and commercial Pt/C catalyst in 0.5 methanol + 0.5 M H_2SO_4 mixture on 0.6 V; (c) CO stripping voltammograms study of BDP@Pt composites in 0.5 M H_2SO_4 electrolyte solution with scan speed 50 mV^{-1}.

oxidation of CO to CO_2 at room temperature [41,42]. With increasing the Pt-NPs loading density, the number of available active site is increased and it is significantly reflected on the methanol oxidation reaction.

4. Conclusion

In the conclusion, we have successfully developed surfactant free, very small Pt-NPs by a simple, clean room temperature, solution dipping method for high performance fuel cell catalyst toward methanol oxidation reaction. Preparation method has been employed through a red-ox reaction between BDP tubes and Pt-based salt to make of BDP@Pt composite. BDP tubes itself acts as a reducing agent as well as template cum stabilizing agent for Pt-NPs formation at room temperature. The Pt-NP loading density on BDP tubes varies with w/w ratio of BDP to Pt-salt. Prepared BDP@Pt composites are showing good CO-tolerance properties with Pt-NPs loading density due to presence of BDP as a template helps for catalytic methanol oxidation reaction. Among four BDP@Pt composites, BDP@Pt3 is the best with respect to efficiency and CO-tolerance ability for the repeated cycles.

Acknowledgements

Dr. S. Malik acknowledges CSIR, India (Project No.: 02(0161)/13/EMR-II) for the financial support. S. Mondal is indebted to CSIR, New Delhi, India for his fellowship. Thanks to Dr. A. Mondal, IACS, Kolkata and Mr. S. Dutta, IITKGP, Kolkata for scientific discussion. We are thankful to the Unit of Nanoscience (DST, Government of India) at IACS, Kolkata, for FEGTEM and XPS.

Appendix A. Supplementary data

Supplementary data related to this article can be found at http://dx.doi.org/10.1016/j.jpowsour.2016.08.026.

References

[1] B.C.H. Steele, A. Heinzel, Nature 414 (2001) 345–352.
[2] C. Bianchini, P.K. Shen, Chem. Rev. 109 (2009) 4183–4206.
[3] N. Kakati, J. Maiti, S.H. Lee, S.H. Jee, B. Viswanathan, Y.S. Yoon, Chem. Rev. 114 (2014) 12397–12429.
[4] Y.L. Hsin, K.C. Hwang, C.-T. Yeh, J. Am, Chem. Soc. 129 (2007) 9999–10010.
[5] A.B.A.A. Nassr, I. Sinev, M.-M. Pohl, W. Grünert, M. Bron, ACS Catal. 4 (2014) 2449–2462.
[6] M. Winter, R. Brodd, Chem. Rev. 104 (2004) 4245–4269.
[7] H. Huang, Q. Chen, M. He, X. Sun, X. Wang, J. Power Sources 239 (2013) 189–195.
[8] B. McNicol, D. Rand, K. Williams, J. Power Sources 83 (1999) 15–31.
[9] F. Ren, H. Wang, C. Zhai, M. Zhu, R. Yue, Y. Du, P. Yang, J. Xu, W. Lu, ACS Appl. Mater. Interfaces 6 (2014) 3607–3614.
[10] X. Wang, C. Li, G. Shi, Phys. Chem. Chem. Phys. 16 (2014) 10142–10148.
[11] M. Liu, Y. Lu, W. Chen, Adv. Funct. Mater 23 (2013) 1289–1296.
[12] A.U. Nilekar, K. Sasaki, C.A. Farberow, R.R. Adzic, M. Mavrikakis, J. Am. Chem. Soc. 133 (2011) 18574–18576.
[13] Y.–J. Gu, W.-T. Wong, Langmuir 22 (2006) 11447–11452.
[14] L.-X. Ding, A.-L. Wang, G.-R. Li, Z.-Q. Liu, W.-X. Zhao, C.-Y. Su, Y.-X. Tong, J. Am. Chem. Soc. 134 (2012) 5730–5733.
[15] S. Zhou, T. Schultz, M. Peglow, K. Sundmacher, Phys. Chem. Chem. Phys. 3 (2001) 347–355.
[16] R. Dillon, S. Srinivasan, A. Arico, V. Antonucci, J. Power Sources 127 (2004) 112–126.
[17] Y. Li, W. Gao, L. Ci, C. Wang, P.M. Ajayan, Carbon 48 (2010) 1124–1130.
[18] Y. Mu, H. Liang, J. Hu, L. Jiang, L. Wan, J. Phys. Chem. B 109 (2005) 22212–22216.
[19] B.E. Hayden, Acc. Chem. Res. 46 (2013) 1858–1866.
[20] Y. Xia, Y. Xiong, B. Lim, S.E. Skrabalak, Angew. Chem. Int. Ed. 48 (2009) 60–103.
[21] Y. Shen, Z. Zhang, R. Long, K. Xiao, J. Xi, ACS Appl. Mater. Interfaces 6 (2014) 15162–15170.
[22] A. Mondal, N.R. Jana, ACS Catal. 4 (2014) 593–599.
[23] H. Huang, S. Yang, R. Vajtai, X. Wang, P.M. Ajayan, Adv. Mater 26 (2014) 5160–5165.
[24] G. Zhang, C. Huang, R. Qin, Z. Shao, D. An, W. Zhang, Y. Wang, J. Mater. Chem. A 3 (2015) 5204–5211.
[25] L. Shi, R.-P. Liang, J.-D. Qiu, J. Mater. Chem. 22 (2012) 17196–17203.
[26] Y. Zhou, G. Yang, H.-B. Pan, C. Zhu, S. Fu, Q. Shi, D. Du, X. Cheng, J. Yang, C.M. Wai, J. Mater. Chem. A 3 (2015) 8459–8465.
[27] A. Santasalo-Aarnio, M. Borghei, I.V. Anoshkin, A.G. Nasibulin, E.I. Kauppinen, V. Ruiz, T. Kallio, Int. J. Hydrogen Energy 37 (2012) 3415–3424.
[28] E.S. Steigerwalt, G.A. Deluga, C. Lukehart, J. Phys. Chem. B 106 (2002) 760–766.
[29] N. He, C. Qin, R. Wang, S. Ma, S. Ma, Y. Wang, T. Qi, RSC Adv. 6 (2016) 68989–68996.
[30] C.-Z. Li, Z.-B. Wang, X.-L. Sui, L.-M. Zhang, D.-M. Gu, S. Gu, J. Mater. Chem. A 2 (2014) 20139–20146.
[31] T. Maiyalagan, T.O. Alaje, K. Scott, J. Phys. Chem. C 116 (2012) 2630–2638.
[32] H. You, F. Zhang, Z. Liu, J. Fang, ACS Catal. 4 (2014) 2829–2835.
[33] B. Narayanamoorthy, K.K.R. Datta, M. Eswaramoorthy, S. Balaji, ACS Catal. 4 (2014) 3621–3629.
[34] H.S. Kolla, S.P. Surwade, X. Zhang, A.G. MacDiarmid, S.K. Manohar, J. Am. Chem. Soc. 127 (2005) 16770–16771.
[35] D. Li, J. Huang, R.B. Kaner, Acc. Chem. Res. 42 (2009) 135–145.
[36] S. Mondal, U. Rana, S. Malik, ACS Appl. Mater. Interfaces 7 (2015) 10457–10465.
[37] U. Rana, K. Chakrabarti, S. Malik, J. Mater. Chem. 22 (2012) 15665–15671.
[38] P. Xu, X. Han, B. Zhang, Y. Du, H.-L. Wang, Chem. Soc. Rev. 43 (2014) 1349–1360.
[39] W.M. Lemke, R.B. Kaner, P.L. Diaconescu, Inorg. Chem. Front. 2 (2015) 35–41.
[40] B.J. Gallon, R.W. Kojima, R.B. Kaner, P.L. Diaconescu, Angew. Chem. Int. Ed. 46 (2007) 7251–7254.
[41] Z. Yang, M.R. Berber, N. Nakashima, J. Mater. Chem. A 2 (2014) 18875–18880.
[42] A.-L. Wang, H. Xu, J.-X. Feng, L.-X. Ding, Y.-X. Tong, G.-R. Li, J. Am. Chem. Soc. 135 (2013) 10703–10709.
[43] H. Gharibi, M. Amani, H. Pahlavanzadeh, M. Kazemeini, Electrochim. Acta 97 (2013) 216–225.
[44] S. Mondal, S.U. Rana, S. Malik, Chem. Commun. 51 (2015) 12365–12368.
[45] U. Rana, S. Mondal, J. Sannigrahi, P.K. Sukul, M.A. Amin, S. Majumdar, S. Malik, J. Mater. Chem. C 2 (2014) 3382–3389.
[46] H. Huang, X. Wang, J. Mater. Chem. A 2 (2014) 6266–6291.
[47] U. Rana, K. Chakrabarti, S. Malik, J. Mater. Chem. 21 (2011) 11098–11100.
[48] R.-X. Wang, J.-J. Fan, Y.-J. Fan, J.-P. Zhong, L. Wang, S.-G. Sun, X.-C. Shen, Nanoscale 6 (2014) 14999–15007.
[49] S. Dutta, C. Ray, A. Mondal, S.K. Mehetor, S. Sarkar, T. Pal, Electrochim. Acta 159 (2015) 52–60.
[50] H. Tsunoyama, H. Sakurai, N. Ichikuni, Y. Negishi, T. Tsukuda, Langmuir 20 (2004) 11293–11296.
[51] B. Yue, Y. Ma, H. Tao, L. Yu, G. Jian, X. Wang, X. Wang, Y. Lu, Z. Hu, J. Mater. Chem. 18 (2008) 1747–1750.
[52] S. Mondal, U. Rana, R.R. Bhattacharjee, S. Malik, RSC Adv. 4 (2014) 57282–57289.
[53] S.K. Meher, G.R. Rao, ACS Catal. 2 (2012) 2795–2809.
[54] A.L.M. Reddy, S. Ramaprabhu, J. Phys. Chem. C 111 (2007) 16138–16146.
[55] M. Yang, Q. Cai, C. Liu, R. Wu, D. Sun, Y. Chen, Y. Tang, T. Lu, J. Mater. Chem. A 2 (2014) 13738–13743.
[56] J. Yang, C. Tian, L. Wang, H. Fu, J. Mater. Chem. 21 (2011) 3384–3390.
[57] B.Y. Xia, H.B. Wu, X. Wang, X.W. Lou, J. Am. Chem. Soc. 134 (2012) 13934–13937.
[58] Z.Q. Tian, S.P. Jiang, Y.M. Liang, P.K. Shen, J. Phys. Chem. B 110 (2006) 5343–5350.
[59] X. Yang, X. Liu, X. Meng, X. Wang, G. Li, C. Shu, L. Jiang, C. Wang, J. Power Sources 240 (2013) 536–543.
[60] Y. Zhao, L. Fan, H. Zhong, Y. Li, S. Yang, Adv. Funct. Mater 17 (2007) 1537–1541.